

Kondo effect and absence of quantum interference effects in the charge transport of cobalt doped iron pyrite

S. Guo,¹ D.P. Young,¹ R.T. Macaluso,² D.A. Browne,¹ N.L. Henderson,¹ J.Y. Chan,² L.L. Henry,³ and J.F. DiTusa¹

¹*Department of Physics and Astronomy, Louisiana State University, Baton Rouge, Louisiana 70803 USA*

²*Department of Chemistry, Louisiana State University, Baton Rouge, Louisiana 70803 USA*

³*Department of Physics, Southern University, Baton Rouge, Louisiana, 70813 USA*

(Dated: June 24, 2018)

The Hall effect and resistivity of the carrier doped magnetic semiconductor $\text{Fe}_{1-x}\text{Co}_x\text{S}_2$ were measured for $0 \leq x \leq 0.16$, temperatures between 0.05 and 300 K, and fields of up to 9 T. Our Hall data indicate electron charge carriers with a density of only 10 to 30% of the Co density of our crystals. Despite the previous identification of magnetic Griffiths phase formation in the magnetic and thermodynamic properties of this system for the same range of x , we measure a temperature independent resistivity below 0.5 K indicating Fermi liquid-like transport. We also observe no indication of quantum corrections to the conductivity despite the small values of the product of the Fermi wave vector and the mean-free-path, $1.5 \leq k_F \ell \leq 15$, over the range of x investigated. This implies a large inelastic scattering rate such that the necessary condition for the observation of quantum contributions to the carrier transport, quantum coherence over times much longer than the elastic scattering time, is not met in our samples. Above 0.5 K we observe a temperature and magnetic field dependent resistivity that closely resembles a Kondo anomaly for x less than that required to form a long range magnetic state, x_c . For $x > x_c$, the resistivity and magnetoresistance resemble that of a spin glass with a reduction of the resistivity by as much as 35% in 5 T fields. We also observe an enhancement of the residual resistivity ratio by almost a factor of 2 for samples with $x \sim x_c$ indicating temperature dependent scattering mechanisms beyond simple carrier-phonon scattering. We speculate that this enhancement is due to charge carrier scattering from magnetic fluctuations which contribute to the resistivity over a wide temperature range.

PACS numbers: 71.30.+h, 72.15.Gd, 72.15.Qm, 72.15.Rn

I. INTRODUCTION AND MOTIVATION

There has been enormous interest^{1,2,3,4,5,6,7} over the past decade in systems that can be tuned via pressure, magnetic field, or composition, to be in proximity to zero temperature phase transitions, or quantum critical points, QPC. This interest stems from the non-standard, or non-Fermi liquid, NFL, behavior commonly found^{1,2,3,4,5,6,7,8,9} in metals near QCP's. Many of the systems investigated, particularly those that are tuned by way of chemical substitution, are significantly disordered and the role of the disorder in determining the physical properties is not well understood^{10,11,12,13,14,15}. Recent theoretical work^{11,12,13,14,15} has focused on the emergence of Griffiths phases in disordered materials where statistically rare regions of order, or disorder, can dominate the thermodynamic response. This appears particularly relevant near zero temperature phase transitions where the formation of Griffiths phases in disordered metals is thought to be the cause of the NFL behavior observed over wide regions of composition, temperature and magnetic field.

In a previous paper¹⁶ we presented, and in the accompanying article¹⁷ expand upon, the magnetic and thermodynamic properties of the magnetic semiconductor $\text{Fe}_{1-x}\text{Co}_x\text{S}_2$ which displays features consistent with the formation of Griffiths phases^{13,14}. We have demonstrated the formation of clusters of magnetic moments both at low temperatures for x less than x_c , the critical

concentration for a long ranged magnetic ground state, as well as at temperatures above the critical temperature, T_c , for $x > x_c$. Here, T_c is defined as the temperature where the real part of the AC susceptibility displays a maximum (see Ref. [17]). In the temperature range where these clusters form we find power-law temperature, T , and magnetic field, H , dependencies with small exponents in agreement with that predicted for Griffiths phases.

Here, we investigate in more full detail the charge transport properties of these compounds to explore the consequences of Griffiths phase formation. We find that the Co substitution induces metallic behavior with a small density of electron-type carriers in all of our Co doped crystals, including our most lightly doped ($x = 3 \times 10^{-4}$). For samples with $x \leq x_c$ the resistivity, ρ , and magnetoresistance, MR, are consistent with Kondo scattering of the carriers^{18,19,20,21,22,23}. That is, we observe a logarithmically decreasing $\rho(T)$ and a $\rho(T, H)$ that scale as $(\rho - \rho(H = 0)) / \rho(H = 0) = f[H / (T + T^*)]$, where T^* is the Kondo temperature and $\rho(H = 0)$ the zero field resistivity. As we increase x beyond x_c we find that magnetic ordering produces an increasing $\rho(T)$ up to temperatures somewhat above T_c , similar to what is observed in metallic spin glasses²⁴. The application of a magnetic field of 5 T dramatically reduces the resistivity of these samples by up to 35% at low temperatures. In this way the system resembles common metals with magnetic impurities with Kondo behavior seen at low impurity concentrations

and a decreasing ρ with decreasing T below a spin glass temperature for higher impurity concentrations^{23,24}.

As is true of nearly all metals that display Kondo anomalies, the resistivity of our $\text{Fe}_{1-x}\text{Co}_x\text{S}_2$ crystals displays Fermi liquid behavior at temperatures well below T^* ^{19,23,25}. Here, we observe a temperature independent resistivity below 0.5 K for samples having both $x \leq x_c$ as well as those with $x > x_c$. The main difference between our crystals and common Kondo systems is that $\text{Fe}_{1-x}\text{Co}_x\text{S}_2$ has a small density of charge carriers and poor conduction in the range of x that we investigate. A typical figure of merit for transport in disordered metals is $k_F\ell$, where k_F is the Fermi wave vector and ℓ is the mean-free-path of the charge carriers. Here, $k_F\ell$ is between 1.5 and 15 for $3 \times 10^{-4} \leq x \leq 0.1$ a range typical of doped semiconductors in proximity to the insulator-to-metal (IM) transition where quantum contributions to the conductivity are expected^{26,27}. Quantum interference effects, such as the electron-electron interaction effects^{26,27} described by Altshuler, are expected under the conditions of diffusive transport and low temperatures such that the elastic scattering time for carriers is much shorter than the time required to randomize the charge carrier's quantum phase. Under these conditions a square-root singularity in the electronic density of states is thought to form, resulting in a \sqrt{T} and \sqrt{H} dependent conductivity^{28,29,30}. Measurements in doped semiconductors, including some magnetic semiconductors, display the typical signatures of electron-electron interaction effects, including the positive MR and a distinctive scaling of the conductivity in H/T ^{28,30,31}. We observe none of these standard behaviors of disordered Fermi liquid behavior, instead finding a negative MR and a temperature independent conductivity at $T < 500$ mK, despite the small values of $k_F\ell$ that we infer.

The absence of quantum interference effects in the conductivity of our samples is puzzling. We point out, however, that there is reason to believe that the charge carriers have a substantial inelastic scattering rate even at the lowest temperatures we measure. The high density of low lying magnetic excitations associated with the magnetic Griffiths phases that we have identified in this system are likely to provide a large inelastic scattering cross-section for the charge carriers, even at temperatures well below 1 K^{16,17}. We speculate that the condition for observation of the quantum corrections to the conductivity, that the carriers retain quantum coherence over times much longer than the inelastic scattering time^{26,27}, is not met in our samples because of the magnetic scattering. Reduction of the magnetic scattering by application of magnetic fields as large as 9 T does not appear sufficient to restore the quantum interference effects as the resistivity continues to be T independent even at such large fields.

Beyond the surprising lack of quantum interference effects, we observe no indication of NFL behavior in the transport properties of our $\text{Fe}_{1-x}\text{Co}_x\text{S}_2$ crystals. Thus, just as in the prototypical semiconducting systems such as phosphorous doped silicon^{32,33,34}, NFL behavior ob-

served in the magnetic and thermodynamic properties that persist into the metallic side of the IM transition, does not lead to NFL charge transport. In Si:P, where disordered Fermi liquid transport is observed³², the implication is that the conducting electrons and the more localized dopants which dominate the magnetization and specific heat, C , only interact weakly. It has even been postulated that these two electron fluids reside in physically separate regions of the disordered semiconductor. In contrast, in $\text{Fe}_{1-x}\text{Co}_x\text{S}_2$, we find convincing evidence that the conducting electrons and the localized electrons responsible for the magnetic properties of these materials interact substantially. The Kondo resistance anomaly, so clearly defined in our data, indicates the importance of such an interaction. Yet, surprisingly, we do not observe any indication of NFL behavior in the charge carrier transport to the lowest temperatures measured despite ample evidence for NFL response of $M(H, T)$ and $C(H, T)$ ^{16,17}.

There are several other peculiarities that we observe in our samples with Co concentrations closest to the critical concentration for the nucleation of a finite temperature long range magnetic phase. First, we have measured a very large anomalous Hall coefficient, R_S , for samples with x near x_c . R_S becomes much smaller as x is increased. The magnitude of R_S does not appear to scale with the resistivity of our samples in the manner predicted by the accepted models^{35,36,37} of the anomalous Hall effect. In addition, we observe a residual resistivity ratio, RRR, defined as the resistivity at 300 K divided by the resistivity at 4 K, that is nearly 2 for all samples except those with x near x_c , where it is almost twice as large. This indicates that there is an additional temperature dependent scattering mechanism beyond the typical phonon induced carrier scattering of common metals^{38,39}. We demonstrate that fits of the Bloch model for phonon scattering in metals do not completely describe $\rho(T)$ for samples with $x \sim x_c$. Instead, we find that a simple AT^α dependence with $\alpha \sim 1.5$, describes $\rho(T)$ well over a large temperature range. The success of this simple form in modeling our data suggests that magnetic fluctuation scattering may be important over a wide T range for samples in proximity to a zero temperature phase transition^{1,4,5,7,8,40,41,42}.

The purpose of this article is to provide a more full rendering of our Hall effect, resistivity, and magnetoresistance data and analysis than that published previously¹⁶. In addition, we emphasize here the absence of quantum contributions to the low temperature transport that was not included in our previous work.

This paper is organized as follows: We outline some of important experimental details of the sample preparation, the initial characterization, and the measurement techniques in section II. This is followed by a presentation of our Hall effect data and analysis. The resistivity and magnetoresistance of our $\text{Fe}_{1-x}\text{Co}_x\text{S}_2$ crystals is presented in section III B. Finally we summarize our results in section IV.

II. EXPERIMENTAL DETAILS

Single crystals of $\text{Fe}_{1-x}\text{Co}_x\text{S}_2$ were synthesized from high purity starting materials, including Fe powder (Alfa Aesar 99.998%), Co powder (Alfa Aesar 99.998%), and sulfur (Alfa Aesar 99.999%) as described previously^{16,17}. Initial characterization included single crystal X-ray diffraction as described in Refs.16,17. The lattice constant determined by the X-ray diffraction experiments¹⁷ showed a systematic increase with Co concentration, x , in $\text{Fe}_{1-x}\text{Co}_x\text{S}_2$, beyond the lattice constant for pure FeS_2 , $a = 0.54165$ nm and consistent with the measurements of Ref.43. The increase in lattice constant with x is consistent with Vegard's law and the idea that Co replaces Fe within the pyrite crystal structure. Energy-dispersive X-ray microanalysis (EDX) on JEOL scanning electron microscope equipped with a Kevex Si(Li) detector was performed to check the stoichiometry of our samples and were found to be consistent with the magnetic moment density determined by our DC magnetization measurements¹⁷. Because magnetization measurements were easily performed and highly reproducible, we have subsequently used the saturated magnetization to determine the Co concentration of our samples. Thus, throughout this manuscript the stoichiometry of the samples noted in the figures and text was determined in this manner. The variations in the saturated magnetization for crystals from the same growth batch was measured to be $\pm 10\%$ of the average value. Therefore, we report x determined from measurements of M at high field for the crystals used in each of our measurements. Wherever possible, the same crystal was employed for several different measurement types, particularly for the Hall effect and magnetization measurements used to determine anomalous Hall coefficients. As described in the accompanying article, the AC susceptibility was used to establish the magnetic phase diagram identifying Curie temperatures, T_c , and the critical Co concentration for formation of a magnetic ground state, $x_c = 0.007 \pm 0.002$ ^{16,17}.

Resistivity, magnetoresistance (MR), and Hall effect measurements were performed on single crystals polished with emery paper to an average size of 0.5 mm x 1 mm x 0.1 mm. Thin Pt wires were attached to four contacts made with Epotek conductive silver epoxy. Hall effect measurements were performed at 17 or 19 Hz on samples with carefully aligned voltage leads in a Quantum Design MPMS gas flow cryostat from 1.8 to 300 K. These measurements were done in a superconducting magnet with fields ranging from -5 to 5 T and the Hall voltage, V_H , was determined as $V_H = [V(H) - V(-H)]/2$, to correct for any contamination from the field symmetric MR due to misalignment of the contacts. The resistivity and MR measurements were performed at 17 or 19 Hz using standard lock-in techniques in the Quantum Design MPMS gas flow cryostat with a 5 T superconducting magnet and a dilution refrigerator equipped with a 9 T superconducting magnet.

III. EXPERIMENTAL RESULTS

A. Hall Effect

We begin our discussion of the transport properties of the charge carriers donated by the Co substitution by presenting our Hall effect measurements which give us an estimate of the charge carrier densities in our crystals. In Fig. 1a the Hall resistivity, ρ_{xy} , is plotted for 3 representative samples including our $x = 0.0007$ sample (at 1.8 K), our $x = 0.007$ sample (at 1.8 and 10 K), and our $x = 0.045$ sample at a series of temperatures between 1.8 and 300 K. All samples display a negative ρ_{xy} , indicating n-type carriers, except at low fields and temperatures where a positive Hall potential is found for samples with $x \geq x_c$. This large positive contribution to ρ_{xy} at low fields, demonstrated in the figure for our $x = 0.007$ and $x = 0.045$ samples, is suppressed with temperature so that by warming to 10 K we again find a negative $\rho_{xy}(H)$ which is linear in H . The observation of a low-field positive contribution to ρ_{xy} is not surprising since magnetic materials typically have two contributions to their Hall resistivities, an ordinary part due to the Lorentz force experienced by the carriers proportional to H and inversely proportional to the carrier density, and an anomalous part proportional to the sample's magnetization. It is common to parameterize ρ_{xy} as

$$\rho_{xy} = R_0 H + 4\pi M R_S \quad (1)$$

with R_0 the ordinary Hall coefficient, R_S the anomalous Hall coefficient, and M the magnetization, to highlight these contributions^{35,36,37}. Interest in the anomalous Hall effect has grown over the past few years because of the large contribution it makes to ρ_{xy} in magnetic semiconductors^{37,44,45,46,47}. The present understanding of the anomalous Hall effect includes contributions from extrinsic sources, due to spin-orbit scattering, and intrinsic sources, from spin-orbit effects inherent in the material's band structure^{35,37}. These theories predict a strong dependence of R_S on the carrier scattering rate such that $R_S \propto \rho_{xx}^2$ for intrinsic or side jump scattering and $R_S \propto \rho_{xx}$ for skew scattering dominated transport^{36,37}.

As is standard practice, we display in Fig. 1b the quantity ρ_{xy}/H as a function of $4\pi M/H$ where M is the measured magnetization of these same crystals. Plotting the data in this way allows a comparison of our measured ρ_{xy} with Eq. 1. In the case where the ordinary Hall coefficient is field independent, as it is for a single carrier band, a linear M/H dependence is often found. Here we see significant curvature to ρ_{xy} indicating that there are either multi-band effects in R_0 , or that there is a field dependence to the anomalous coefficient. Field dependent R_S values are observed in materials having large MRs since the carrier scattering rates are field dependent⁴⁸. However, such an analysis was not successful in modeling the M/H dependence of ρ_{xy}/H shown in Fig. 1b. A significant temperature dependence of R_S is also apparent for our $x = 0.045$ sample in Fig. 1b.

R_S values for our samples that are very close to the critical point for magnetic ordering.

FIG. 1: (Color online) Hall resistivity. a) The Hall resistivity, ρ_{xy} , vs magnetic field, H , at several temperatures, T , for 3 representative crystals with T 's and x 's identified in the figure. Note that the ρ_{xy} scale for the $x = 0.045$ sample is on the right-hand-side of the figure. b) ρ_{xy}/H plotted as a function of the magnetization, M , divided by H to highlight the anomalous part of the Hall resistivity. Symbols the same as in frame a. The line is a fit of a $\rho_{xy}/H = R_0 + R_S(4\pi M/H)$ form to the $x = 0.045$ data at 1.8 K with R_0 and R_S fitting parameters taken to be independent of H . Inset: Same as frame b for $x = 7 \times 10^{-4}$ and $x = 0.007$ samples on a smaller scale. Line is a linear fit, same form as in the main frame of the figure, to the $x = 0.007$ data at 4 K.

The results of parameterizing ρ_{xy} as in Eq. 1 are shown in Fig. 2 where R_0 and R_S are plotted as a function of T for five samples including the same three samples displayed in Fig. 1. R_S for our $x = 0.0007$ crystal was omitted from the figure because ρ_{xy} is highly linear and the magnetization of this sample too small to allow an accurate determination. The T -dependence of both R_0 and R_S that were apparent in Fig. 1a and b are made quantitative with the use of this simple form for the Hall resistivity. What is interesting, first, is the observation of significant temperature dependencies of the Hall coefficients below 10 K where the magnetic susceptibility, specific heat, and, as we demonstrate below, ρ all display unusual behavior associated with the magnetic properties of these materials^{16,17}. Second, we find very large

FIG. 2: (Color online) Temperature dependence of the Hall coefficients. a) The ordinary Hall coefficient, R_0 , as a function of temperature, T , for five representative crystals with x identified in the figure. R_0 is determined from fits of the Hall resistivity to the standard form $\rho_{xy} = R_0H + 4\pi MR_S$ where M is the measured magnetization and R_S is the anomalous Hall coefficient. b) Temperature dependence of R_S for 4 crystals identified in frame a. R_S determined with the same procedure as in frame a.

The x dependence of R_S and R_0 for a large number of crystals is presented in Fig. 3. Here we demonstrate the very large values of R_S found near x_c along with a continuous decrease with x beyond x_c . We note that neither the standard extrinsic nor intrinsic theories of the anomalous Hall coefficient can explain the x dependence of R_S that we measure here by way of a scattering rate variation with x . As we demonstrate in the discussion of the conductivity below, we measure very small variation in ρ over the range in x where the large decrease in R_S is apparent in Fig. 3a. At present, we do not have an adequate understanding of the very large values of R_S we measure near x_c , although we speculate that an inhomogeneous magnetic state, the Griffiths phase, for $x \sim x_c$ identified from our magnetic and thermodynamic measurements, may amplify the anomalous Hall effect near

x_c ^{16,17}. In frame *c* of the figure we plot the carrier density calculated from the simple form $R_0 = 1/n_{Hall}ec$, where n_{Hall} is the carrier density, e is the electronic charge, and c is the speed of light. We observe that n_{Hall} increases with Co substitution although it is much smaller than the Co density of these crystals, particularly for $x > 0.025$. Our values of n_{Hall} indicate a carrier concentration of only 10 to 30% of the Co density. Thus, there appears to be significant fraction of the electrons added by the Co substitution that are in localized states.

FIG. 3: (Color online) Cobalt concentration dependence of the Hall coefficients and carrier density. a) Cobalt concentration, x , dependence of the anomalous Hall coefficient, R_S at 1.8 K. R_S was determined from fits of the form $\rho_{xy} = R_0H + 4\pi MR_S$ to the Hall resistivity, ρ_{xy} , where R_0 is the ordinary Hall coefficient. b) x dependence of R_0 determined from the same fits at 1.8 and 300 K as identified in frame a. c) Carrier concentration, n_{Hall} determined from the simple form for the ordinary Hall coefficient, $R_0 = 1/n_{Hall}ec$, where e is the electronic charge and c is the speed of light, at 1.8 and 300K as identified in frame a. Dashed red line represents the carrier concentration expected if each Co dopant were to donate a single electron to a conducting band.

Our Hall data have established the sign of the charge carriers, negative as expected for Co substitution in FeS₂, and that the carrier density is only 10 to 30% of the Co density of our crystals. In addition, we find very large Hall conductivities resulting from extraordinarily large anomalous Hall coefficients for samples close to the critical concentration for magnetism.

B. Conductivity

After establishing that our crystals were single phase and that Co successfully replaces Fe in FeS₂ adding electron-like carriers, we determined the conductivity σ of our samples. Fig. 4 shows that, although the nominally pure FeS₂ crystal is insulating, all of our crystals with Co substitutions were metallic having a conductivity that extrapolates to a non-zero value at $T = 0$ ⁴⁹. Further, our crystals have σ that increases with x for $x \leq 0.035$ and decrease for larger x . These trends are made clearer in Fig. 5 where we plot the residual resistivity defined as $\rho_0 = \sigma^{-1}$ at $T = 1.8$ K. Since the Hall effect measurements presented in section III A display a continuous increase in n_{Hall} with x for $x < 0.025$ followed by a relatively constant carrier density at larger x , the decreased σ at $x > 0.035$ indicates that the Co impurities, or other substitution dependent defects, represent strong scattering centers for the carriers. The conductivity decreases with T over most of the temperature range also indicating metallicity for all $x > 0$. We summarize the T -dependence of σ by plotting the residual resistivity ratio, RRR, of our crystals in the inset to Fig. 5. Here RRR is defined as ratio of the resistivity, $\rho = 1/\sigma$, at 300 K to that at 4 K and the figure demonstrates that RRR is shown to be between 1.9 and 4 for all of our $x > 0$ samples. Metals with small disorder typically display a large RRR due to a strongly T -dependent scattering rate for charge carrier-phonon scattering below the Debye temperature ($\Theta_D = 610$ K for FeS₂)^{50,51}. For disordered metals this dependence can be hidden by a large impurity, T -independent, scattering rate. In our samples, the RRR is small, a second indication that the impurities and defects related to the chemical substitution represent strong scattering centers for the doped carriers. In addition to the temperature independent impurity related scattering and the T -dependent phonon scattering apparent in the conductivity, there appears to be a separate, T -dependent, contribution to the conductivity of our crystals evident below ~ 20 K.

1. Resistivity Below 20 K

The temperature dependence of the charge carrier transport at low temperatures can often reveal much about the character of the charge carriers and their scattering. Therefore we have explored the carrier transport below 20 K in some detail as shown in Figs. 6 and 7 where we display the resistivity of a few representative crystals. As these figures demonstrate, crystals with $x < 0.01$ generally display a decreasing ρ with T below 20 K, while those with $x > 0.01$ display an increasing ρ with T leading to a maximum in ρ at temperatures somewhat above T_c ¹⁷. In addition, we observe that ρ tends toward saturation by $T < 0.3$ K, a behavior typically observed in metals without substantial disorder where it is indicative of transport in a Fermi liquid. The resistivities we

FIG. 4: (Color online) Conductivity. a) and b) Temperature, T , and cobalt concentration, x , dependence of the electrical conductivity, σ , of several representative crystals. The stoichiometry of the crystals is identified in the figure.

FIG. 5: (Color online) Residual resistivity and residual resistivity ratio. The residual resistivity, ρ_0 , (resistivity at 1.8 K) of our $\text{Fe}_{1-x}\text{Co}_x\text{S}_2$ crystals. Inset; Residual resistivity ratio, RRR, defined as the resistivity at 300 K divided by ρ_0

measure are above $500 \mu\Omega \text{ cm}$, consistent with the small carrier concentration revealed in our Hall effect measurements and a large scattering rate. A typical measure of the proximity to the insulator-to-metal transition is the quantity $k_F\ell$, where k_F is the Fermi wave vector and ℓ is the mean-free-path of the carriers. Our estimates of $k_F\ell$ at 4 K for the samples shown in Fig. 4 range from 1.5 for our smallest x , to 15 for the crystals having the

smallest ρ_0 in Fig. 5. With $k_F\ell$ being close to 1, it is generally expected that ρ display evidence of electron-electron interaction effects that dominate the low- T magnetotransport of prototypical semiconductors^{26,27,28}, and some magnetic semiconductors^{31,52}, near the IM transition. The conductivity of common semiconductors with doping concentrations near that required for a IM transition displays both a $T^{1/2}$ dependence at low- T and a positive MR that grows as $H^{1/2}$ for $g\mu_B H > k_B T$. We show below that we observe neither of these signatures of disordered Fermi-liquid transport in $\text{Fe}_{1-x}\text{Co}_x\text{S}_2$. In this same range of x and T , our specific heat and magnetic susceptibility measurements reveal the formation of Griffiths phases which have been suggested to be a cause of non-Fermi liquid behavior^{11,13,16,17}. Instead, we observe a temperature independent resistivity below 1 K with no indication of quantum interference effects in the carrier transport. The coincidental observation of the formation of an interesting disordered magnetic phase and the absence of quantum interference in the electrical conductivity suggests that the scattering of carriers from magnetic excitations associated with the Co dopant ions is substantially inelastic. This large inelastic scattering rate may be sufficient to cut off any quantum interference effects associated with the diffusive transport of the carriers.

FIG. 6: (Color online) Resistivity and Magnetoresistance. a) through d) Temperature, T , dependence of the resistivity, ρ of four single crystals at magnetic fields, H , and stoichiometry's identified in the figure. Zero field data same as in Fig. 4. Solid line is a fit of a Kondo anomaly form to the data using the Kondo temperature determined from a scaling of the magnetoresistance data (see text)¹⁹.

As is apparent in Figs. 6 and 7 the application of magnetic fields substantially decreases ρ for all samples measured, independent of the sign of $d\rho/dT$. The decrease in resistivity is as large as 35% of ρ_0 for a 5 T field. The negative MR we observe is at odds with what has been measured in common semiconductors such as Si:P, and other magnetic semiconductors, such as $\text{Fe}_{1-x}\text{Co}_x\text{Si}$, where a positive MR is associated with the electron-

FIG. 7: (Color online) Low temperature resistivity. The resistivity, ρ , as a function of temperature, T , at $0.07 < T < 20$ K for two representative crystals. Stoichiometry and magnetic fields are identified in the figure. Dashed line is a fit of the Kondo form¹⁹ to the data for a $x = 0.005$ crystal above 0.5 K with the Kondo temperature held at 1.4 K as determined from the best scaling of the magnetoresistance data. See text for details.

electron interaction effects^{28,30,31}. For samples that display a $d\rho/dT < 0$ at $H = 0$ the effect of magnetic field is to reverse the sign of the temperature derivative so that all samples have a $d\rho/dT > 0$ at high fields. Instead of resembling the transport of charge carriers in prototypical semiconductors, we observe a behavior similar to what is seen when magnetic impurities are added to high purity metals²³.

In common metals the addition of magnetic impurities leads to a low temperature resistivity anomaly that has been extensively investigated^{18,23} for over 40 years. Small impurity densities, typically less than 0.01%, induce an increased resistivity with decreasing T similar to what we observe here. This is the well known Kondo effect^{18,23} where conduction electrons increasingly screen the magnetic impurities as the temperature is lowered. The effect of a magnetic field is to Zeeman split the energy levels of the impurity moments effectively removing the Kondo resonance, thereby removing a scattering channel for the carriers. At higher impurity concentrations, interactions between impurity magnetic moments become of the same order as the effective screening temperature, $k_B T^*$, where T^* is the Kondo temperature and k_B is Boltzmann's constant. In this case, a spin glass or a disordered magnetic state forms at low- T and is typically indicated by a decrease in ρ below the glass freezing or magnetic ordering temperature²⁴. We note that the T and x ranges where we observe $d\rho/dT > 0$ at $H = 0$ correspond well with the magnetically ordered states identified by a peak in the AC susceptibility¹⁷.

In Figs. 6 and 7 we have included a comparison of our data for $\rho(T)$ at $H = 0$ with a standard form for the

Kondo resistance anomaly given by Hamann^{19,20}

$$\rho_{spin} = S\rho_0 \left(1 - \cos 2\delta_\nu \frac{\ln T/T_K}{(\ln^2 T/T_K + \pi^2 S(S+1))^{1/2}} \right), \quad (2)$$

where T_K is the Kondo temperature, S the spin of the impurity, δ_ν the phase shift due to ordinary scattering, and ρ_0 the s-wave unitarity limit resistivity. We have fit this form to our data for $x < x_c$ with S set at 1/2 and T_K held at the value of T^* found from the scaling of the MR, see below, and found best fit values for δ_ν between 25 and 60°.

The field dependence of ρ at constant T for the same 4 crystals as in Fig. 6 is shown in Fig. 8 where the negative MR is once again displayed. The size of the MR decreases with temperature so that by about $T = 25$ K there is only a small MR (< 5%). The MR at 1.8 K is large indicating that the scattering of the carriers by the magnetic impurities is dominating the resistivity of our crystals, particularly at larger x . We also observe a change in the shape of the MR at low H for $x > 0.01$. Although the MR is negative and analytic at $H = 0$ for samples with $x < x_c = 0.007 \pm 0.002$, as well as for $x > x_c$ at $T > T_c$, it is very sharp at $T < T_c$, a feature commonly observed in ferromagnetic metals⁵³.

FIG. 8: (Color online) Magnetoresistance. a) through d) The magnetoresistance (resistivity, ρ as a function of magnetic field, H) for the same crystals as in Fig. 6 with stoichiometry's and temperatures, T , identified in the figure. The current direction was perpendicular to H , transverse MR, for all data presented in the figure.

A common indicator for the mechanism of the MR is the difference in MR for currents parallel and perpendicular to the magnetic field. In Fig. 9 we plot the MR measured for two representative samples in the two current-field configurations. We have chosen one sample with $x < x_c$ and one with $x > x_c$ for this plot, and in both cases there is little change in the MR with field orientation. We conclude that the contributions to the MR from orbital effects is minimal in agreement with our tentative assignment of the MR, and T -dependent ρ , to a Kondo anomaly.

To further test the hypothesis that the MR is related to scattering from magnetic moments associated with the

FIG. 9: (Color online) Transverse and longitudinal magnetoresistance. a) The magnetoresistance, MR, defined as the resistivity, ρ , as a function of magnetic field, H after subtracting the resistivity at $H = 0$, ρ_0 , and dividing by ρ_0 , $\rho - \rho_0/\rho_0$, of two representative crystals at 1.8 K. Stoichiometry's of the crystals are identified in the figure. The longitudinal MR refers to the current direction being parallel to H . The transverse MR refers to the measurement geometry where the current is in the same direction with respect to the crystal as in the longitudinal MR measurement, but with the crystal oriented such that the current is perpendicular to H .

Co substitution, and more specifically the Kondo effect for $x < x_c$, we have attempted a simple scaling of the MR to a standard Kondo form, $(\rho - \rho_0)/\rho_0 = f(H/(T + T^*))$ ^{21,22}. In Fig. 10 we display the typical results of our scaling procedure for crystals with $0.004 \leq x \leq 0.16$. While the scaling quality is within the scatter of the data for paramagnetic samples, $x < x_c = 0.007$, there is significant deviation from scaling for samples having a magnetic transition at finite T . The values for T^* resulting in the best scaling of our data are plotted in Fig. 11 where T^* is seen to increase with x . We conclude from the quality of the scaling of the data that a single ion Kondo form does well to describe the resistivity where the interaction between moments is expected to be small, that is, for $x \leq x_c$ and T larger than a scale related to the interactions between local moments, such as an RKKY energy scale. This is in accord with our magnetization measurements for samples with $x < x_c$ where the T dependence of the magnetic susceptibility displays a small negative Weiss T ^{16,17}. From the quality of the fits shown in the figures, and the quality of the scaling of the MR in Fig. 10, we conclude that a single ion Kondo form describes the low temperature transport of our samples with $x < x_c$ well, while for $x > x_c$ the transport properties resemble those of Kondo systems where the concentration of magnetic impurities is large enough so that interaction between them results in magnetic ordering.

FIG. 10: (Color online) Scaling plot of the magnetoresistance. a) through d) Magnetoresistance, $\rho - \rho_0/\rho_0$ where ρ is the resistivity and ρ_0 refers to the resistivity in zero magnetic field, H , as a function of H divided by the temperature, T , added to the Kondo temperature, T^* determined by the best scaling of these data. The stoichiometry of the crystals is indicated in the figure, as is the value of T^* which leads to the best scaling of the data. T and H for the constant temperature and field scans are indicated in the figure. The scaling is seen to work well for samples where $x < x_c$, the critical Co concentration for ferromagnetism, frames a and b. In frames c and d where $x > x_c$, no value of T^* results in reasonable scaling of all the data.

FIG. 11: (Color online) Kondo temperature. The Co concentration dependence, x of the Kondo temperature T^* as determined from scaling of the magnetoresistance, see Fig. 10 for example. Only samples where x is less than the critical concentration for ferromagnetism, x_c , is T^* accurately determined and only those data are plotted in the figure.

2. Resistivity above 20 K

Above 20 K the conductivity shown in Fig. 4 decreases with increased T demonstrating metallic conduction of the carriers introduced by Co substitution. However, the thermally induced scattering does not decrease the conductivity of our crystals by more than a factor of 2 in

most crystals (see RRR in Fig. 5) reflecting the importance of the substitutional disorder.

The resistivity of a few representative samples is shown in Fig. 12 (a) and (b) where the temperature dependence of the resistivity appears to be almost linear over a wide range of temperatures. In the usual description of metallic transport, based in part on Matthiessen's rule, carrier scattering due to impurities is considered temperature independent, while the scattering from the thermally activated phonons is highly T -dependent. The standard^{38,39}, semiclassical, Debye treatment of carrier-phonon scattering predicts a $\rho \propto (T/\Theta_D^\rho)^5$ behavior for $T < \Theta_D^\rho$ evolving into a $\rho \propto T/\Theta_D^\rho$ form for $T > \Theta_D^\rho$. Here Θ_D^ρ is the transport Debye temperature. The Debye temperature for iron pyrite is 610 K⁵⁰ and we estimate the transport Debye temperature, $\Theta_D^\rho = 2\hbar k_F s/k_B$, where s is the speed of sound (8980 m/s), to be between 200 and 250 K^{39,54}. To test if the resistivity we measure in $\text{Fe}_{1-x}\text{Co}_x\text{S}_2$ can be described as being due to carrier scattering from phonons, we have fit the full Debye form to our data. We have included a Kondo form, Eq. 2, consistent with the the low- T data, to our model in order to accurately model the resistivity at $T < 20$ K. In this procedure we have varied the impurity resistivity, ρ_0 , the carrier mass enhancement, and Θ_D^ρ , while keeping the carrier density fixed to the value determined from the Hall effect measurements and assuming a spherical Fermi surface to estimate k_F , in order to find the best representation of our data. The results of this procedure are shown in Fig. 12 a and b by the solid lines. The difference between the data and model is presented as a percentage of the measured resistivity in frame c of the figure, and the best fit values of Θ_D^ρ displayed in frame d. Best fit values of the carrier mass ranged between 1 and 1.5 times the bare electron mass. From the quality of the fits shown in the figure, we conclude that the semiclassical treatment adequately describes the resistivity of our samples over a wide range of T with a few notable exceptions and qualifications. The first, as is apparent in frame c of the figure, is that the model does not accurately describe the behavior below 100 K. In particular, for samples with x close to x_c , the model deviates substantially from the data near 50 K. In addition, the values of Θ_D^ρ determined from our fitting procedure for crystals with $x < x_c$ are much larger than the Debye temperature of pure FeS_2 which would be surprising if true.

We have considered a simple alternative to the standard phonon scattering model of resistivity motivated by our observation that the resistivity data appear to have a nearly linear T -dependence over a wide range in T . This alternative, demonstrated in Fig. 13, consists of a simple power-law form, $\rho = \rho_0 + AT^\alpha$, added to the same Kondo description of the low- T data (Eq. 2) as in Fig. 12. The results of this procedure where α , A , and ρ_0 are allowed to vary is represented in frames a and b of Fig. 13 by the dashed lines. The ability of such a simple model to reproduce the data is remarkable. In fact, the difference between the data and model shown in frame c of Fig. 13

FIG. 12: (Color online) Temperature dependence of the resistivity; Bloch model. a) The resistivity, ρ for 3 crystals with Co concentrations, x indicated in the figure. Solid lines are fits of the Bloch model of lattice resistance^{38,39} to our data. The model includes a residual resistivity, ρ_0 added to a Kondo anomaly determined from fits to the low temperature resistivity ($T < 10\text{K}$) for example see Fig. 6 and displayed below 150 K by the dotted lines in the figure. b) ρ for 5 representative crystals with x 's indicated in the figure. Dashed and dotted lines are the same as in frame a. c) $\rho - \rho_f/\rho$, deviation of the resistivity from the fits, ρ_f . d) Transport Debye temperature, Θ_D^ρ as determined from fits of the model to the data in frame a and b.

is smaller for samples with $x \sim x_c$ than the much more complex Debye model of Fig. 12, although some systematic differences remain below 100 K. The best fit values of the temperature exponent, α , are shown in frame d where α is seen to change from about 2.5 for small x ($x = 3 \times 10^{-4}$) to values between 1.2 and 1.6.

Why such a simple expression does such an accurate job of describing our resistivity data is not clear. However, we suggest that the formation of a magnetically ordered state at low- T implies that scattering from magnetic fluctuations plays an important role in determining $\rho(T)$. The large reduction of the residual resistivity by the application of moderately sized magnetic fields, a decrease of 45% of ρ_0 with a 9 T field as seen in Fig. 8, supports the idea that magnetic scattering is a substantial fraction of ρ_0 . Our observation that the $\text{RRR} \approx 4$ for samples near x_c , along with the observation that the Debye model for carrier scattering from phonons has systematic differences with the data, and the quality of fits of a simple power law temperature dependence to $\rho(T)$, all indicate magnetic fluctuations to be an important contribution to the carrier scattering in this range of x over a wide temperature range.

The simple power-law analysis of $\rho(T)$ at $T > 20$ K has demonstrated that the resistivity of our samples closely resembles a $\rho = \rho_0 + AT^\alpha$ dependence with $\alpha \approx 1.5 \pm 0.1$ in a wide range of x and T . In order to assess the sys-

FIG. 13: (Color online) Temperature dependence of the resistivity; power-law model a) The resistivity, ρ for 3 crystals with Co concentrations, x indicated in the figure. Dashed lines are fits of a model that includes a residual resistivity, ρ_0 added to a Kondo anomaly and a simple power law form, AT^α . The Kondo form was determined from fits to the low temperature resistivity ($T < 10K$) for example see Fig. 6 and displayed below 150 K by the dotted lines in the figure. b) ρ for 5 representative crystals with x 's indicated in the figure. Dashed and dotted lines are the same as in frame a. c) $\rho - \rho_f / \rho$, deviation of the resistivity from the fits, ρ_f , showing that for crystals with x in proximity to x_c a power law form with $\alpha = 1.6 \pm 0.1$ describes the data well over an extended temperature range. d) α as determined from fits of the model to the data in frame a and b.

tematics and validity of this model we have plotted the quantity $(\rho - \rho_0)/(\rho_0 * T^{1.5})$ in Fig. 14. In this way we can compare scattering rates in samples with very different carrier concentrations, and remove the error associated with the measurement of the geometry of our crystals. If the power-law expression were to strictly hold, this quantity would yield the parameter A divided by the residual resistivity. Dividing by ρ_0 normalizes A by eliminating the simple effects of carrier concentration and impurity scattering rate changes with x . Thus, the figure isolates the magnitude of this quantity related to the T -dependent part of the scattering rate of the carriers. The figure demonstrates that this value is very closely clustered about $(\rho - \rho_0)/(\rho_0 T^{1.5}) = 2 \times 10^{-4} \text{ K}^{-1.5}$ for nearly all of our samples. The obvious exceptions are the crystals with x nearest to x_c on the paramagnetic side where a value of $(\rho - \rho_0)/(\rho_0 T^{1.5}) = 4 \times 10^{-4}$ to $6 \times 10^{-4} \text{ K}^{-1.5}$ is found, reflecting the observation of a much larger RRR in these samples.

It appears from this simple analysis that the T -dependent scattering rate above $\sim 150 \text{ K}$ is extraordinarily independent of x for $x > x_c$ while is at least twice as large for $x \simeq x_c$. From this we conclude that there is a carrier scattering mechanism that is enhanced very near the critical concentration for magnetism in this system.

Given the power-law like dependence on T , we assert that carrier scattering from magnetic fluctuations contributes a significant fraction of the resistivity over the entire temperature range we measure.

FIG. 14: (Color online) Reduced resistivity. a) The resistivity, ρ , after subtraction of the resistivity at 4 K, ρ_0 , normalized by ρ_0 and divided by $T^{1.5}$ vs. temperature, T , for 14 representative crystals with x 's identified in the figure. All samples except those with x nearest to x_c have values that approach $2 \times 10^{-4} \text{ K}^{-1.5}$ while those with $x \sim x_c$ display values larger than $4 \times 10^{-4} \text{ K}^{-1.5}$. The red line in the figure represents a linear temperature dependence, such as that expected for phonon scattering at T larger than the Debye temperature.

Resistivities, and thus by implication charge carrier scattering rates, that display similar temperature dependent power law behaviors for $T < 20 \text{ K}$ have been documented for nearly ferromagnetic and weakly ferromagnetic metals such as $\text{Pd}_{1-x}\text{Ni}_x$ ⁴⁰ and ZrZn_2 ⁴, where scattering from spin fluctuations produces a $T^{5/3}$ dependence of ρ . This behavior is observed in highly itinerant magnets where a Stoner-Wholfarth model of magnetism⁴² is appropriate and is thought to signify the emergence of a marginal Fermi liquid ground state⁵⁵. A second group of materials well known for having power-law T -dependent resistivities, $\rho = \rho_0 + AT^\alpha$, with small α , for $T < 10K$, are those near quantum critical points (QCP), such as a zero- T magnetic critical point. Examples include MnSi under pressure^{2,5}, $\text{Ce}(\text{Cu}_{1-x}\text{Au}_x)_6$ ⁷, and YbRh_2Si_2 ¹. None of these examples display power-law behavior above about 20 K. One exception is the high temperature superconducting oxides of copper where $\rho \propto T^{1.5}$ has been documented for over-doped samples of $\text{La}_{2-x}\text{Sr}_x\text{CuO}_4$ over an enormous temperature range⁸. How the temperature dependent resistivity of $\text{Fe}_{1-x}\text{Co}_x\text{S}_2$ we observe here fits into this evolving story is not clear. However, we point out that all of these materials reside near a magnetic phase transition that has been tuned toward zero temperature.

A simple picture that can explain the $T^{1.5}$ temperature dependence is to assume that the electrons are scattered by spin wave excitations of the disordered system. These spin waves are the excitations around the Griffiths phase ordered state. We assume that the density of states of

spin waves in the disordered system varies as \sqrt{E} as it does in a clean system, despite the fact that the spin waves do not have a well defined momentum. In calculating the scattering of an electron we include all spin wave energies up to about $k_B T$, leading to a net scattering rate that varies as $T^{1.5}$. Because the spin excitations have no well defined momentum, even low energy scattering events can result in large momentum changes for the electron, so the transport lifetime is similar to the single particle lifetime, unlike the case in clean materials where the phonon scattering varies as T^5 instead of T^3 because of the momentum conservation in the scattering. This scattering process will persist well above the Curie temperature, as it does in clean materials where neutron scattering typically sees a well defined spin wave peak even for temperatures well above the onset of order.

IV. DISCUSSION AND CONCLUSIONS

In $\text{Fe}_{1-x}\text{Co}_x\text{S}_2$ we have previously observed that the Co dopants each contribute localized magnetic moments to the slightly diamagnetic insulator FeS_2 ^{16,17,49}. These moments tend to form magnetic clusters and at low T we have observed the emergence of a disordered ferromagnetic phase at $x_c = 0.007 \pm 0.002$. Our Hall effect data presented here reveal a density of electrical carriers of only 10 to 30% of the Co concentration indicating a substantial localization of electrons donated by the Co substitution. A slight curvature evident in the plots of the Hall potential vs. the magnetic field may indicate the existence of a small population of compensating holes. The reasons for the low carrier densities is not clear at this time but may reflect a significant substitutional-related disorder. In the magnetically ordered samples we observe an anomalous Hall effect with a very large coefficient (R_S) which decreases with x .

Measurements of the low- T conductivity show that the charge carriers interact substantially with the magnetic moments in this system. We have presented evidence that the Kondo effect dominates the carrier transport for $x \leq x_c$ for $T < 10$ K and, as is the case for both simple metals with magnetic impurities and Kondo lattice systems^{19,23,25}, the resistivity saturates at low T . We point out that the carrier densities estimated from the Hall effect are sufficient to screen only a small fraction of the doping induced magnetic moments, leaving the system highly underscreened or undercompensated. The temperature independent ρ at the lowest T 's indicate a Fermi liquid ground state with contributions from quantum interference effects commonly observed in doped semiconductors surprisingly absent.

The usual indicator for the observation of quantum contributions to the conductivity, $k_F \ell$ is well within the range where such effects are expected in our data. The reason for the absence of such contributions is not completely clear. We speculate that the charge carrier inelastic scattering rate does not become much smaller than the

elastic scattering rate at low temperatures as is required for the observation of quantum effects. The source of the inelastic scattering most likely involves the magnetic degrees of freedom associated with the nearly magnetically ordered (for $x < x_c$), or the spin-glass-like or disordered ferromagnetic, phase (for $x > x_c$). As we have asserted previously, the disorder associated with the chemical substitution leads to the formation of a magnetic Griffiths phase which may provide an enormous density of low energy excitations and a source for inelastic scattering for the charge carriers. The application of a magnetic field substantially decreases the resistivity of our $\text{Fe}_{1-x}\text{Co}_x\text{S}_2$ crystals at low- T ^{21,22}. This is typical of magnetic materials since the field gaps the low frequency magnetic fluctuation spectrum and removes much of the inelastic carrier scattering. Despite the decreased scattering with the application of magnetic fields, we still do not observe any quantum interference effects.

The low temperature transport properties of $\text{Fe}_{1-x}\text{Co}_x\text{S}_2$ we outline above are substantially different from those of Co and Mn substituted FeSi, a second magnetic semiconducting system where detailed low- T measurements have been carried out^{31,44,52}. While both of the nominally pure compounds, FeS_2 and FeSi, have small band gaps and are nonmagnetic having very small magnetic susceptibilities, both become magnetic upon electron doping via Co substitution. However, electron doping of FeSi results in a highly itinerant helimagnetic ground state where standard quantum contributions to the conductivity are dominant. Clearly this is distinct from what we measure here in $\text{Fe}_{1-x}\text{Co}_x\text{S}_2$. Hole doping FeSi by way of Mn substitution is similar to $\text{Fe}_{1-x}\text{Co}_x\text{S}_2$ in that it was found to display undercompensation⁵². Here, the Mn dopants contribute a spin-1 moment and a single spin-1/2 hole carrier. The resistivity of these compounds remained T -dependent down to the lowest temperatures, however, the temperature dependence was not the $T^{1/2}$ behavior found in standard semiconducting systems such as Si:P^{28,30}. The NFL behavior discovered in $\text{Fe}_{1-x}\text{Mn}_x\text{Si}$ is in agreement with calculations predicting a singular Fermi liquid in the undercompensated Kondo model^{56,57,58,59}. In addition, the application of modest magnetic fields reduces the inelastic scattering and restores the typical temperature and field dependencies expected for quantum interference effects³¹. We remain puzzled as to the cause of dramatic differences in the transport properties of these, naively similar, magnetic semiconducting systems.

Finally, the temperature dependence of the resistivity in the T -range where phonon scattering dominates the ρ of typical metals shows some peculiarities. In particular, the temperature dependence of the resistivity is enhanced for samples with x very near x_c , having a RRR twice as large as samples on either side of x_c . Although a semiclassical model of carrier-phonon scattering describes the broad features of $\rho(T)$ our models show systematic differences with the data below 100 K for the samples with

$x \sim x_c$. We have demonstrated that a simple power-law form surprisingly describes the data at least as well as the semiclassical model^{38,39} in this range of x . We speculate that the resistivity of these compounds results, in part, from magnetic fluctuation scattering of the carriers, even at temperatures approaching room T .

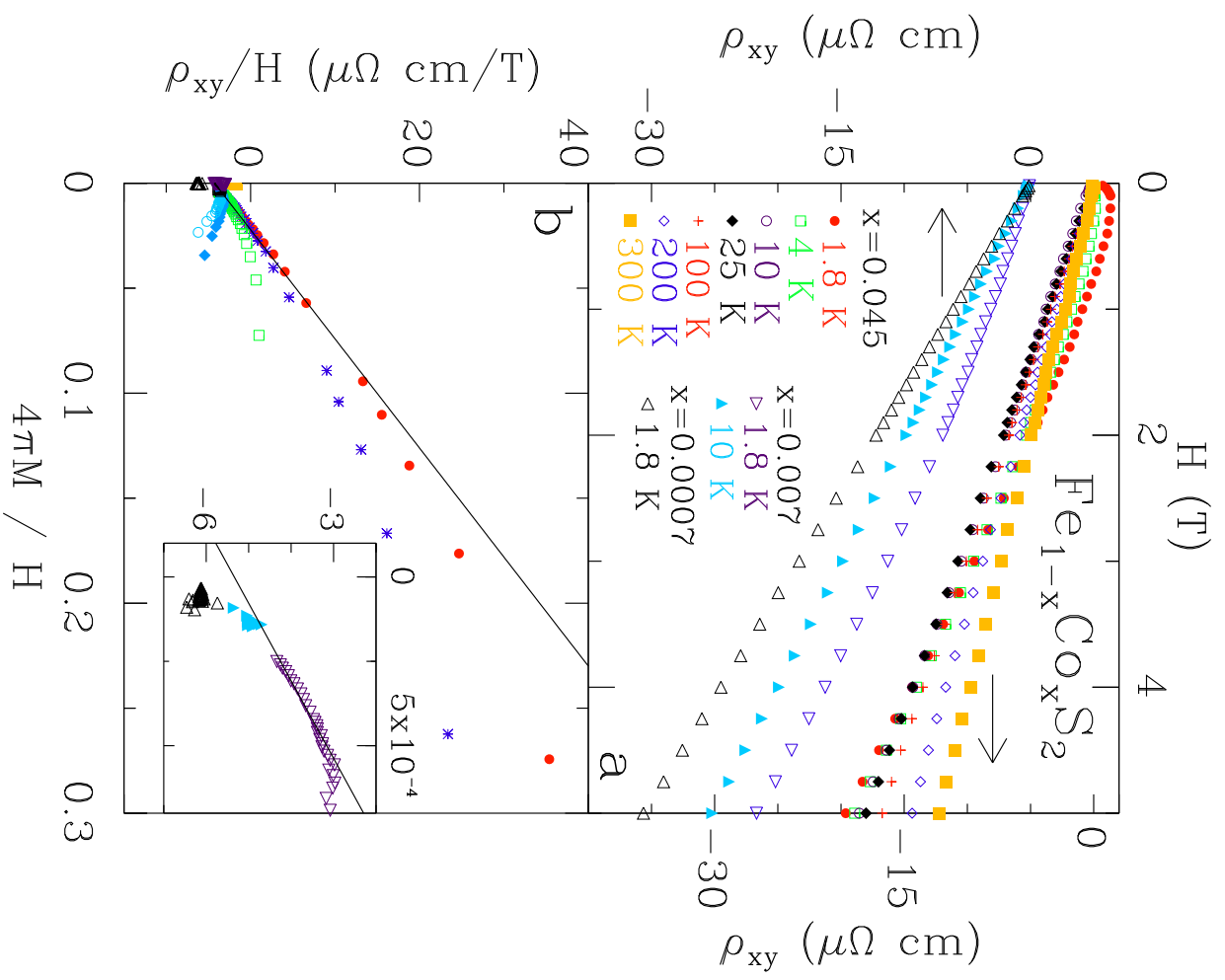
In summary, Co doping of FeS₂ adds both local magnetic moments and electron charge carriers to this band gap insulator. Our data indicate that although the magnetic and thermodynamic properties of Fe_{1-x}Co_xS₂ for $0 \leq x \leq 0.085$ are dominated by the presence of Griffiths phases at low temperatures, the transport is Fermi liquid like. It appears that there is a Kondo coupling of the car-

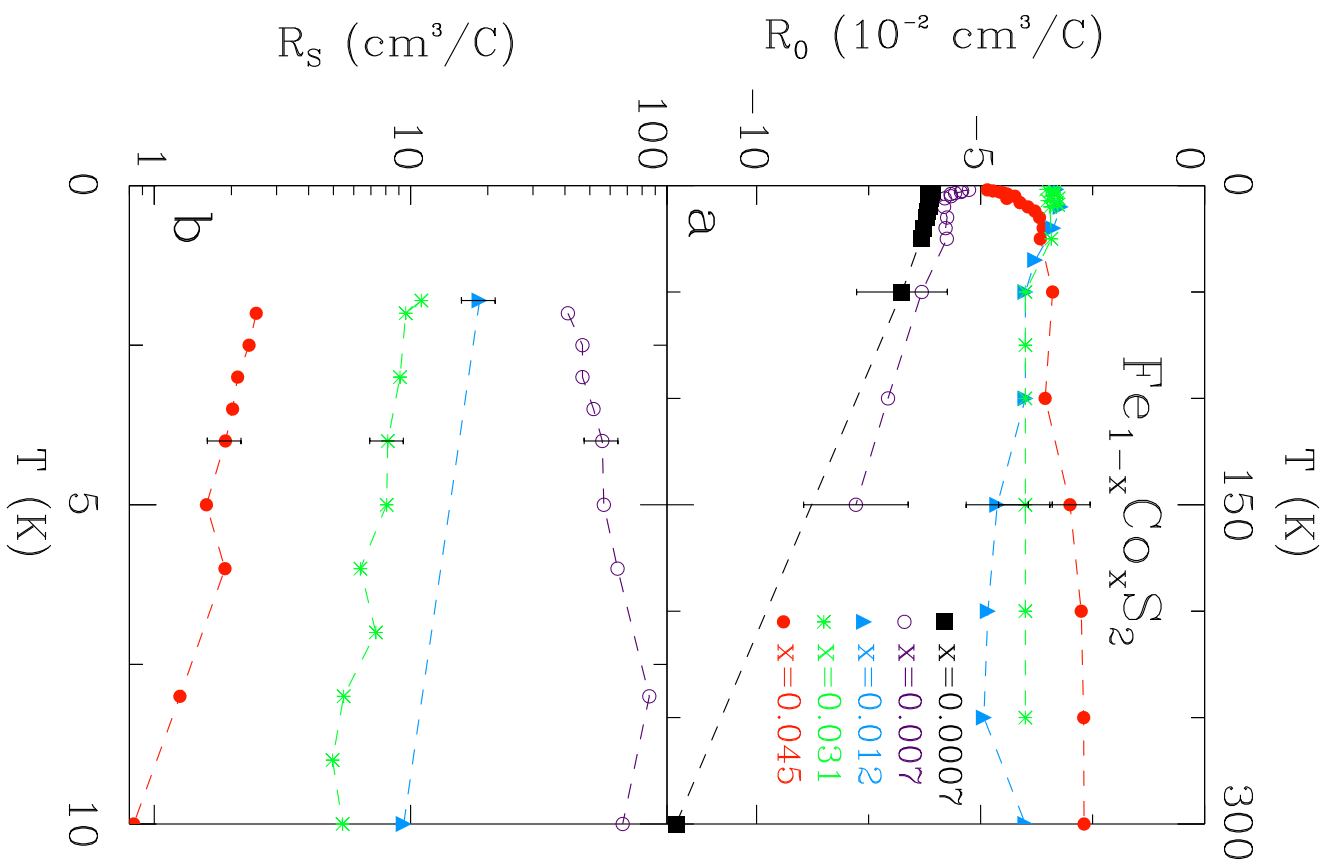
riers and local magnetic moments that produces a temperature independent resistivity below ~ 0.5 K. Despite the small mean-free-path of the doped charge carriers we observe no indication of quantum corrections to the conductivity which we speculate is due to a large inelastic scattering rate of the carriers. Thus, our data indicate that there may be a range over which the inelastic scattering rate is too large for quantum contributions to be observable, and yet too small to induce non-Fermi liquid behavior in the transport of disordered conductors.

We thank I. Vekhter and C. Capan for discussions. JFD, DPY, and JYC acknowledge support of the NSF under DMR084376, DMR0449022, and DMR0756281.

-
- ¹ J. Custers, P. Gegenwart, H. Wilhelm, K. Neumaier, Y. Tokiwa, O. Trovarelli, C. Geibel, F. Steglich, C. Pepin, & P. Coleman, *Nature* **424** 524-527 (2003)
 - ² N. D. Mathur, F. M. Grosche, S. R. Julian, I. R. Walker, D. M. Freye, R. K. W. Haselwimmer, & G. G. Lonzarich, *Nature* **394**, 39-43 (1998).
 - ³ Q. M. Si, K. Ingersent, & J. L. Smith, *Nature* **413**804-808 (2001).
 - ⁴ R.P. Smith, M. Sutherland, G. G. Lonzarich, S. S. Saxena, N. Kimura, S. Takashima, M. Nohara, & H. Takagi, *Nature* **455**, 1220-1223 (2008).
 - ⁵ N. Doiron-Leyraud, I. R. Walker, L. Taillefer, M. J. Steiner, S. R. Julian, & G. G. Lonzarich, *Nature* **425**, 595-599 (2003).
 - ⁶ G. R. Stewart, *Rev. Mod. Phys.* **73**,797-855 (2001)
 - ⁷ A. Schroder, G. Aeppli, R. Coldea, M. Adams, O. Stockert, H. von Lohneysen, E. Bucher, R. Ramazashvili, & P. Coleman, *Nature* **407**, 351-355 (2000).
 - ⁸ H. Takagi, B. Batlogg, H. L. Kao, J. Kwo, R. J. Cava, J. J. Krajewski, & W. F. Peck, *Phys. Rev. Lett.* **69**, 2975-2978 (1992).
 - ⁹ J. S. Kim, J. Alwood, G. R. Stewart, J. L. Sarrao, & J. D. Thompson, *Phys. Rev. B* **64**, 134524 (2001).
 - ¹⁰ R. B. Griffiths, *Phys. Rev. Lett.* **23**,17 (1969).
 - ¹¹ A. H. Castro Neto, G. Castilla, & B. A. Jones, *Phys. Rev. Lett.* **81**,3531-3534 (1998).
 - ¹² A. H. Castro Neto & B. A. Jones, *Phys. Rev. B* **62**, 14975-15011 (2000).
 - ¹³ E. Miranda & V. Dobrosavljevic, *Rep. Prog. Phys.* **68**, 2337-2408 (2005).
 - ¹⁴ T. Vojta, *J. Phys. A:Math. Gen.* **39**, R143-R205 (2006).
 - ¹⁵ A. J. Millis, D. K. Morr, & J. Schmalian, *Phys. Rev. B* **66**, 174433 (2002).
 - ¹⁶ S. Guo, D. P. Young, R. T. Macaluso, D. A. Browne, N. L. Henderson, J.Y. Chan, L.L. Henry, & J.F. DiTusa, *Phys. Rev. Lett.* **100**, 017209 (2008).
 - ¹⁷ S. Guo, D. P. Young, R. T. Macaluso, D. A. Browne, N. L. Henderson, J.Y. Chan, L.L. Henry, & J.F. DiTusa, submitted to *Phys. Rev. B* (2009).
 - ¹⁸ J. Kondo, *Prog. Theor. Phys.* **32**, 37-49 (1964).
 - ¹⁹ D. R. Hamann, *et al.* *Phys. Rev.* **158**, 570-580 (1967).
 - ²⁰ J. S. Schilling, *Adv. Phys.* **28**, 657-715 (1979).
 - ²¹ P. Schlottmann, *Phys. Rep.* **181**, 1-119 (1989).
 - ²² B. Andraka & G. R. Stewart *Phys. Rev. B* **49**, 12359-12361 (1994).
 - ²³ C. Rizzuto, *Rep. Prog. Phys.* **37**, 147-229 (1974).
 - ²⁴ J. S. Schilling, P. J. Ford, U. Larsen, & J. A. Mydosh, *Phys. Rev. B* **14**, 4368-4380 (1976).
 - ²⁵ Z. Fisk, J. L. Sarao, J. L. Smith, & J. D. Thompson, *Proc. Nat. Acad. Sci.* **92**, 6663-6667 (1995).
 - ²⁶ B. L. Al'tshuler, A. G. Aronov, M.E. Gershenson, & Yu. V. Sharvin, *Sov. Sci. Rev. Phys.* **9**, 223-354 (1987).
 - ²⁷ P. A. Lee & T. V. Ramakrishnan, *Rev. Mod. Phys.* **57**, 287-337 (1985).
 - ²⁸ T. F. Rosenbaum, R. F. Milligan, M. A. Paalanen, G. A. Thomas, R. N. Bhatt, & W. Lin, *Phys. Rev. B* **27**, 7509-7523 (1983).
 - ²⁹ T. F. Rosenbaum, R. F. Milligan, G. A. Thomas, P. A. Lee, T. V. Ramakrishnan, R.N. Bhatt, K. DeConde, H. Hess, & T. Perry, *Phys. Rev. Lett.* **47**, 1758-1761 (1981).
 - ³⁰ S. Bogdanovich, P. H. Dai, M. P. Sarachik, V. Dobrosavljevic, & G. Kotliar, *Phys. Rev. B* **55** 4215-4218 (1997).
 - ³¹ N. Manyala, Y. Sidis, J. F. DiTusa, G. Aeppli, D. P. Young, & Z. Fisk, *Nature* **404**, 581-584 (2000).
 - ³² M. A. Paalanen, J. E. Graebner, R. N. Bhatt, & S. Sachdev, *Phys. Rev. Lett.* **61**, 597-600 (1988).
 - ³³ M. A. Paalanen, S. Sachdev, R. N. Bhatt, & A. E. Ruckenstein, *Phys. Rev. Lett.* **57**, 2061-2064 (1986).
 - ³⁴ M. P. Sarachik, A. Roy, M. Turner, M. Levy, D. He, L. L. Isaacs, & R. N. Bhatt, *Phys. Rev. B* **34** 387-390 (1986).
 - ³⁵ J. M. Luttinger, *Phys. Rev.* **112**, 739-751 (1958).
 - ³⁶ F. E. Maranzara, *Phys. Rev.* **160**, 421-429 (1967).
 - ³⁷ T. Jungwirth, Q. Niu, & A. H. MacDonald, *Phys. Rev. Lett.* **88** 207208 (2002).
 - ³⁸ See e.g. J. M. Ziman, *Electrons and Phonons: The Theory of Transport Phenomena in Solids*, (Oxford, London, 1960).
 - ³⁹ V. F. Gantmakher and Y. B. Levinson *Carrier scattering in metals and semiconductors* (North-Holland, Amsterdam, 1987).
 - ⁴⁰ M. Nicklas, M. Brando, G. Knebel, F. Mayr, W. Trinkl, & A. Loidl, *Phys. Rev. Lett.* **82**, 4268 (1999).
 - ⁴¹ C. Pfleiderer, S. R. Julian, & G. G. Lonzarich, *Nature* **414**, 427-430 (2001).
 - ⁴² See e.g. T. Moriya, *Spin fluctuations in itinerant electron magnetism.*, edited by P. Fulde (Springer, Berlin, 1985).
 - ⁴³ R. J. Bouchard, *Mat. Res. Bull.* **3**, 563 (1968).
 - ⁴⁴ N. Manyala, Y. Sidis, J. F. DiTusa, G. Aeppli, D. P. Young, & Z. Fisk, *Nature Materials* **3**, 255-262 (2004).
 - ⁴⁵ H. Ohno, H. Munekata, T. Penney, S. von Molnar, & L. L.

- Chang, Phys. Rev. Lett. **68**, 2664-2667 (1992).
- ⁴⁶ H. Ohno, A. Shen, F. Matsukura, A. Oiwa, A. Endo, S. Katsumoto, & Y. Iye, Appl. Phys. Lett. **69**, 363-365 (1996).
- ⁴⁷ H. Ohno, J. Magn. Magn. Mater. **200**, 110-129 (1999).
- ⁴⁸ M. Lee, Y. Onose, Y. Tokura, & N. P. Ong, Phys. Rev. B **75**, 172403 (2007).
- ⁴⁹ H. S. Jarrett, W. H. Cloud, R. J. Bouchard, S. R. Butler, C. G. Fredric, & J. Gillson, Phys. Rev. Lett. **21** 617 (1968).
- ⁵⁰ R. A. Robie & J. L. Edwards, J. Appl. Phys. **37**, 2659-2663 (1966).
- ⁵¹ J. Kansy, T. J. Panek, & M. Szuszkiewicz, J. Phys. C-Sol. St. Phys. **17** 1585-1593 (1984).
- ⁵² N. Manyala, J. F. DiTusa, G. Aeppli, & A. P. Ramirez, Nature **454**, 976-980 (2008).
- ⁵³ See e.g. I. A. Campbell & A. Fert *Ferromagnetic Materials* Vol. 3 (Ed. E. P. Wohlfarth) 751-804 (North-Holland, Amsterdam, 1982).
- ⁵⁴ M. Kasami, T. Mishina, S. Yamamoto, & J. Nakahara, J. Lumin. **108**, 291-295 (2004).
- ⁵⁵ C. M. Varma, P. B. Littlewood, S. Schmitt-Rink, E. Abrahams, & A. E. Ruckenstein, Phys. Rev. Lett. **63**, 1996-1999 (1989).
- ⁵⁶ P. Coleman & C. Pepin, Phys. Rev. B **68**,220405(R) (2003).
- ⁵⁷ P. Mehta, N. Andrei, P. Coleman, L. Borda, & G. Zarand, Phys. Rev. B **72**, 014430 (2005).
- ⁵⁸ A. Posazhennikova & P. Coleman, Phys. Rev. Lett. **94**, 036802 (2005).
- ⁵⁹ P. D. Sacramento & P. Schlottmann, J. Phys. Condens. Matter **3**, 9687-9696 (1991).





*

